THE JOURNAL OF BIOLOGICAL CHEMISTRY
Vol. 272, No. 15, Issue of April 11, pp. 9661–9670, 1997

Printed in U.S.A.

Analysis of Binding of Cobra Cardiotoxins to Heparin Reveals a New β-Sheet Heparin-binding Structural Motif*

(Received for publication, December 2, 1996)

Alka A. Vyas, Jiann-Jong Pan, Himatkumar V. Patel, Kavita A. Vyas, Chien-Min Chiang, You-Cheng Sheu, Jenn-Kang Hwang‡, and Wen-guey Wu‡

From the Department of Life Sciences, National Tsing Hua University, Hsinchu 30043, Taiwan

Heparin and heparan sulfate have recently been shown to bind to snake cardiotoxin (CTX) and to potentiate its penetration into phospholipid monolayer under physiological ionic conditions. Herein we analyze the heparin-binding domain of CTX using 10 CTXs from Taiwan and African cobra venom. We also performed computer modeling to obtain more information of the binding at molecular level. The results provide a molecular model for interaction of CTX-heparin complex where the cationic belt of the conserved residues on the concave surface of three finger β-sheet polypeptides initiates ionic interaction with heparin-like molecules followed by specific binding of Lys residues near the tip of loop 2 of CTX. The dissociation constants of CTXs differ by as much as 4 orders of magnitude, ranging from ~140 μM for toxin γ to ~20 nM for CTX M3, depending on the presence of Lys residues near the tip of loop 2. High affinity heparin binding becomes possible due to the presence of Arg-28, Lys-33, or the so-called consensus heparin binding sequence of *X*KK*XXX*K*RX* near the tip of the loop. The well defined three-finger loop structure of CTX provides an interesting template for the design of high affinity heparin-binding polypeptides with β-sheet structure. The finding that several cobra CTXs and phospholipase A2 bind to heparin with different affinity may provide information on the synergistic action of the two venom proteins.

Heparin and heparan sulfate (HS)[1] belong to the glucosaminoglycan subclass of glycosaminoglycans (GAGs) and attract special attention because they exhibit greatest structural diversity (1, 2). Many physiological functions, including wound healing, cell attachment and spreading, recruitment of inflammatory cells (chemokines), and regulation of cell proliferation and differentiation (cytokines) are ascribed to them (for reviews, see Refs. 3 and 4). Heparan sulfate proteoglycans are ubiquitous and abound at cell surfaces, wherefrom they control the entry or availability of approaching entities (3, 5). Numerous proteins, such as growth factors (for review, see Ref. 6), antithrombin III (7), phospholipase A2 (PLA2) (8, 9), among others, bind to heparin with dissociation constants ranging from μM to nM. We recently found that CTX A3, a major component of Taiwan cobra venom, with selective cytolytic activity, also binds to heparin and HS under physiological conditions (10).

In view of the growing importance of functional role of heparin binding protein being identified, significant effort has been devoted, but with contradictory results, to elucidate the so-called heparin binding consensus sequence (11). An attempt to identify a heparin binding motif by linearly aligning a broad collection of alleged heparin binding sequences has been made and a consensus, *X*BB*X*B*X* and *X*BBB*XX*B*X* derived (12). Nevertheless, some of the proteins most affected by heparin do not contain this sequence in their heparin binding site (Ref. 13 and references therein). In addition, recent analysis of heparin binding sites of human antithrombin III (14) points to the requirement of Lys residues outside the previously proposed pentasaccharide binding region. This implies that complicated structural features other than simple cluster of basic residues must operate, and a well defined binding motif remains to be elucidated. The recently solved heparin-basic fibroblast growth factor (FGF) co-crystal structure (15) will promote our understanding further.

Cobra venom CTXs are a family of highly homologous, small (~60–62 amino acids), basic, water-soluble, but membrane-active, polypeptides with well defined three-finger loop β-sheet structures (16–20). Also known as cytotoxins, they target a variety of cell types, in particular cardiac myocytes (21, 22). Although their binding to phospholipids is demonstrated (23, 24), lipids alone cannot account for their high specificity. We have recently suggested that sulfated oligosaccharide may be a target of CTX action and that this binding potentiates its penetration into phospholipid membrane (10). The molecular mechanism of this interaction and the amino acid residues involved remain to be determined.

We undertook a study of interaction of 10 CTXs isolated from venom of *Naja atra*,[2] *Naja mossambica* and *Naja nigricollis* with heparin for the following reasons. Cardiotoxins are highly homologous and their three-dimensional structures are superimposable (for review, see Ref. 20). Differing in some cases by as little as one residue, these naturally occurring variants present themselves as a series of readily available basic proteins that might allow establishment of trends underlying the interaction of basic β-sheet proteins with anionic carbohydrates of the cell surface. This approach, though less specific than site-directed mutagenesis, can be directly applicable in understanding the toxicity of cobra venom. For instance, the results of the present study shows that all the toxins, and some PLA2 from the same venom, bind to heparin, albeit with varying avidity. Furthermore, we analyzed heparin-induced conformational change of CTXs by circular dichroism (CD) spectro-

* This work was supported by Grants NSC 85-2113-M-007-035-Y and NSC 85-2113-M-007-029 from National Science Council, Taiwan. The costs of publication of this article were defrayed in part by the payment of page charges. This article must therefore be hereby marked "*advertisement*" in accordance with 18 U.S.C. Section 1734 solely to indicate this fact.

‡ To whom correspondence should be addressed. Fax: 886-3-5715934.

[1] The abbreviations used are: HS, heparan sulfate; CTX, cardiotoxin; PLA2, phospholipase A2; GAG, glycosaminoglycan; FGF, fibroblast growth factor; CD, circular dichroism; MD, molecular dynamics; Tγ, toxin γ; HPLC, high performance liquid chromatography; LMW, low molecular weight; HMW, high molecular weight.

[2] According to recently revised nomenclature for the asiatic cobra, *N. naja*, species (25).

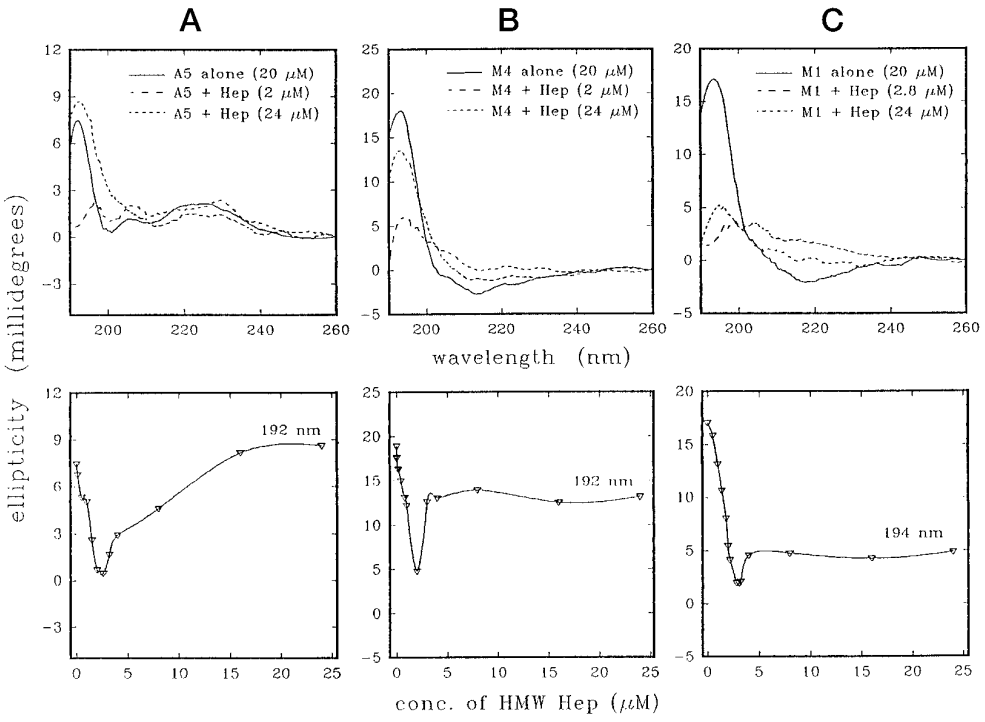

FIG. 1. **HMW heparin-induced structural change in CTXs A5 (*A*), M4 (*B*), and M1 (*C*).** *Top*, representative CD spectra of CTXs, alone and in the presence of heparin, at the indicated concentrations. *Bottom*, ellipticity plotted as a function of concentration of heparin. For CTX A5, the ellipticity of protein with excess sugar rises higher than that for free protein, whereas for M1 it remains considerably low, and for M4 it is intermediate.

scopic and computer molecular dynamic (MD) modeling methods to address the questions of binding motif and stoichiometry of CTX-heparin complex. The proposed model reveals a new type of β-sheet heparin-binding motif with structural feature to explain the high-affinity of three-finger toxins with receptors.

MATERIALS AND METHODS

Crude venom from *Naja naja atra*, *Naja mossambica mossambica* and *Naja nigricollis nigricollis* (according to previous nomenclature) was purchased from Sigma. Heparin (porcine intestinal mucosal) of average M_r 15,000 (HMW heparin) and homolytically depolymerized heparin of average M_r 3,000 (LMW heparin) used in this study were also purchased from Sigma. All other chemicals were of reagent grade. Egg sphingomyelin and phosphatidylcholine were purchased from Avanti Polar Inc. CTXs from *N. atra* and *N. mossambica* venom were purified by SP-Sephadex C-25 ion exchange chromatography and reverse phase HPLC and assayed for hemolytic and fusion activities as described (23, 24). Toxin γ (Tγ) was purified from venom of *N. nigricollis* according to Fryklund and Eaker (26). Purity of CTXs, analyzed by SDS-polyacrylamide gel electrophoresis and analytical reverse phase HPLC, was found to be higher than 99%. Protein concentration was determined by the Lowry method.

Circular Dichroism Measurements—Heparin-induced structural change in CTXs was analyzed by CD spectroscopy. Spectra were recorded on AVIV 62A DS spectropolarimeter (Lakewood, NJ); details of calibration of the spectrometer are reported (19). All experiments were performed in 20 mM sodium phosphate buffer, pH 7.4, due to technical difficulty in monitoring ellipticity at 195 nm using high ionic strength buffer. Typically, 20 μM CTX was titrated against HMW or LMW heparin, and at each point, the solution was incubated for 3 min at room temperature before scanning. Titrations in the reverse order were performed similarly by titrating 20 μM of LMW heparin against CTX. Spectra, average of four repeats, were obtained by scanning from 260 to 190 nm. A 1-mm cell, bandwidth of 1 nm, and time constant of 1 s were used to collect data, reported as ellipticity in millidegrees. Temperature was maintained at 25 °C. Heparin-induced structural perturbation was analyzed according to change in ellipticity around 192–195 nm.

Fluorescence Measurements—Intrinsic fluorescence intensity of Tyr or Trp of CTXs was monitored to determine dissociation constant of the toxins with HMW heparin as reported (10). Briefly, the excitation and emission wavelengths were set at 285 nm and 318 nm for Tyr and at 291 nm and 345 nm for Trp, respectively, by using SLM 4800 fluorescence spectrometer. The dissociation constant, K_d, was determined by nonlinear least squares fitting of data by assuming that n independent, but equivalent, binding sites are present in heparin using the following equation,

$$K_d = ([H_o] - [HC])([C_o] - n[HC])/[HC] \quad \text{(Eq. 1)}$$

where $[C_o]$, $[H_o]$ and [HC] are concentrations of CTX, heparin, and CTX–heparin complex respectively. By using the fluorescence intensity, F, as an indication of the fraction of binding, Equation 1 can be reformulated as the following three equations which can be used to simulate the experimental fluorescence intensity of CTXs as a function of heparin concentration.

$$F_x = F_o + (F_s - F_o)X \quad \text{(Eq. 2)}$$

$$X = (n[H_o] + [C_o] + K_d - Y)/2[C_o] \quad \text{(Eq. 3)}$$

$$Y = \{(n[H_o] + [C_o] + K_d)^2 - 4n[C_o][H_o]\}^{1/2} \quad \text{(Eq. 4)}$$

where F_x is fluorescence intensity and F_o, F_s are intensities when CTX is free and at saturation respectively. Complete (100%) binding was assumed to occur when the fluorescence intensity reached a plateau.

Optical Density Measurements—Change in turbidity of samples was monitored using Beckmann DU-70 spectrophotometer. Typically, CTXs in 20 mM sodium phosphate buffer, pH 7.4, were titrated against LMW heparin and the A_{320} was monitored at each point. In some cases, a reverse titration with constant LMW heparin (20 μM) against increasing CTX concentrations was also studied to reveal the binding mode of CTXs with LMW heparin. The procedure and result are similar to our previous experiment with HMW heparin, but the extent of aggregation as monitored by optical density is in general higher than that detected for HMW heparin.

Heparin Affinity Chromatography—To determine the relative affinities of CTXs, crude venom (3.0–3.8 mg) from *N. atra*, *N. mossambica*, and *N. nigricollis* was loaded onto Heparin-Sepharose column (HiTrap, 1 ml, Pharmacia), fitted to Bio-Rad FPLC system. The column was washed extensively with 10 mM Tris buffer, pH 7.4, and bound fractions were eluted with a linear gradient of 0–1 M NaCl in 10 mM Tris buffer, pH 7.4. The eluted fractions were analyzed for protein concentration by measuring A_{230} using Beckmann DU-70 spectrophotometer. The assignment of respective toxin peaks was done by comparing the HPLC retention times of the fractions with that of purified toxins.

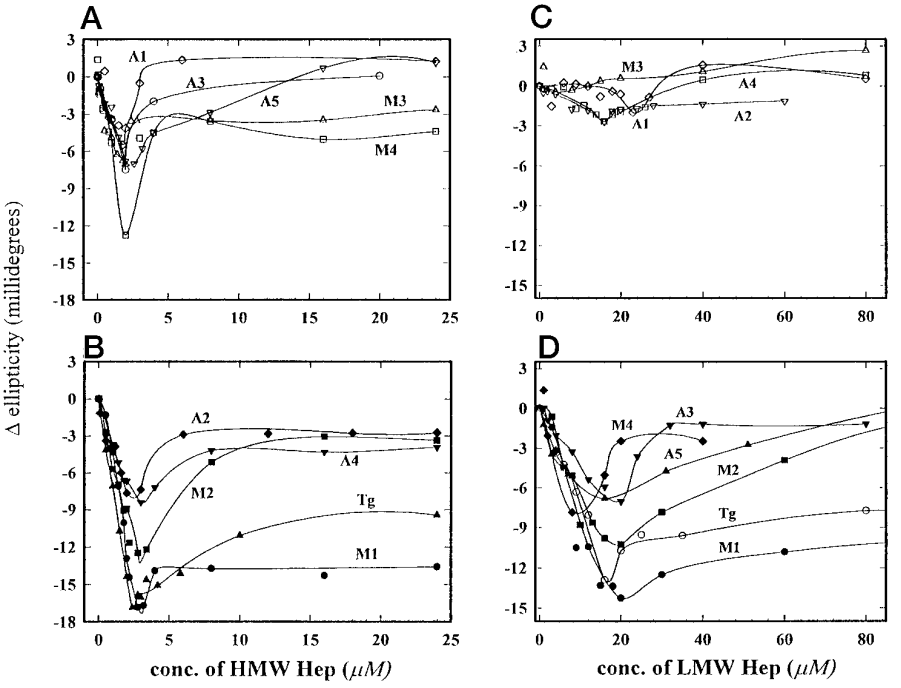

FIG. 2. **HMW and LMW heparin-induced structural change in 10 CTX homologues as studied by change in ellipticity ~195 nm plotted as a function of concentration of the heparin.** CTXs were classified into two groups according to the effective concentration of HMW heparin required to produce maximum structural perturbation in CTX-heparin complex. *A*, effective concentration of heparin for the indicated toxins was around 2 μM. *B*, effective concentration of heparin for the indicated toxins was 2.4–3 μM. CTXs can be classified into two groups according to the extent of LMW heparin-induced conformational change as follows: small change in CD ellipticity, less than 3 millidegrees, of the indicated toxins occurred (*C*) and large change in CD ellipticity, larger than 6 millidegrees, of the indicated toxins was observed (*D*). Ellipticity of free toxin was taken to be 0; hence, the change is negative. Greater values imply larger change. The concentration of CTXs was kept constant at 20 μM.

TABLE I

Comparison of CD ellipticity, effective concentration, and amino acid sequence around loop 2 of CTXs studied with LMW and HMW heparin in 20 mM Na_2HPO_4 buffer

CTX	Amino acid sequence	Θ	Ellipticity[a]						Effective concentration[b] (μM)	
			$\Delta\theta_2$		$\Delta\theta_1$		$\Delta\theta_2 - \Delta\theta_1$			
	20 30 40		LMW	HMW	LMW	HMW	LMW	HMW	LMW	HMW
M1	LCYKMTMRAA **P**-MVPVKRGC	19.1	14.3	16.8	**10**	**13.6**	4.3	3.2	20	2.8
Tg	LCYKMTMRAA **P**-MVPVKRGC	19.3	13.5	16.5	**8.4**	**9.5**	5.1	7.2	16	2.4
M2	LCYKMTMRGA **S**-KVPVKRGC	15.7	10.3	12.5	0.5	3.4	**9.8**	**9.1**	20	2.8
M4	LCYKMTMRLA **P**-KVPVKRGC	17.8	7.9	12.5	2.5	4.4	**5.4**	**8.1**	8	**2**
A3	LCYKMFMVAT **P**-KVPVKRGC	12.5	7.0	7.5	1.2	−0.1	**5.8**	**7.6**	20	**2**
A5	LCFKATLKKF **P**LKFPVKRGC	7.5	6.8	7	−2.7	−1.1	**9.5**	**8.1**	16	2.6
A2	LCYKMFMVSN -LTVPVKRGC	10	**2.7**	7.4	1.1	2.8	1.6	4.6	16	**2**
A4	LCYKMFMVSN -LTVPVKRGC	8.2	**2.7**	8.2	−0.8	3.8	3.5	4.4	16	3
A1	LCYKMFMMSD -LTIPVKRGC	7.2	**2.0**	5.4	−0.6	−1.2	2.6	6.6	23	**1.8**
M3	LCYKMMLASK -KMVPVKRGC	7.8	**0.5**	7	−2.7	2.7	3.2	4.3		**2**

[a] Ellipticity of free CTXs is denoted by θ; total change in ellipticity at maximum perturbation, by $\Delta\theta_2$; change in ellipticity with excess heparin is denoted by $\Delta\theta_1$ and represents the contribution to change, of the first binding site; $\Delta\theta_2 - \Delta\theta_1$ represents contribution of second binding to change. CTX M1 and Tg exhibit higher $\Delta\theta_1$ values and undergo maximum change upon first binding, whereas CTXs M2, M4, A3, A5, exhibit higher $\Delta\theta_2 - \Delta\theta_1$ values and undergo maximum change upon second binding. CTXs A2, A4, A1, and M3 are characterized by low $\Delta\theta_2$ values.

[b] Effective concentration, concentration of heparin required to induce maximum perturbation.

CTX and PLA2 Assays—CTX activity of each fraction was assayed by adding 100 μl aliquots of the fraction to a solution containing 20 mM sphingomyelin vesicles in a total volume of 1 ml 10 mM Tris buffer containing 100 mM NaCl and 1 mM EDTA, pH 7.4, and monitoring the fusion/aggregation activity of the vesicles at A_{450} as described (23). PLA2 activity of eluates was assayed, by adding 100 μl aliquots of each fraction to 4 ml of assay buffer containing 2 mM dimyristoylphosphatidylcholine, 20 mM $CaCl_2$, 10 mM Triton X-100 ml, pH 8.0. The amount of NaOH required to titrate fatty acid released from dimyristoylphosphatidylcholine vesicles, to maintain pH at 8.0, was monitored using Autotitrator (Radiometer, Copenhagen).

Molecular Modeling—The co-ordinates of x-ray structures of CTX A5 were taken from Brookhaven Protein Data Bank and used as the initial structures for molecular modeling. Structure of heparin was obtained from the recently determined structure of hep-bFGF complex (15). Model building, docking and energy minimization were performed on IBM RS6000 375 and Silicon Graphics Indigo II workstation using QUANTA/CHARMM Version 4.0 software. Polar hydrogen atoms were added to the x-ray structures by standard procedure in QUANTA. The initial structures of toxin and heparin were relaxed by energy-minimization to remove initial nonbonded contacts.

Docking of the molecules was performed by using the Modeling Module of QUANTA/CHARMM. Heparin was docked on the concave side of the CTX A5 molecules as indicated by the aggregation property of CTXs (see results). Comparison of the binding strengths of CTXs determined at various ionic strengths suggests that two basic residues, Arg/Lys-28 and Lys-33, are involved in binding. Further optimization of electrostatic interaction allows CTX to be docked in an orientation perpendicular to the three antiparallel β-sheet strand. The docked complex structures were energy-minimized and then subjected to molecular dynamics (MD) simulation. MD simulation was performed with distance-dependent dielectric constant. A time step of 1 fs was used. The nonbonded cutoff value was set at 15 Å, and the nonbonded pair list was updated every 20 time steps. Typical simulation time for each complex was ~40 ps. The final structures generated by MD simulations were energy-minimized and used for analysis. We also carried out preliminary reference MD simulations with explicit all-atom solvent molecules to ensure that our simulation was consistent with that performed in solution.

RESULTS

Interaction of CTXs with HMW Heparin—CTXs exhibit a sharp positive band near 195 nm and weak negative minimum near 215 nm, characteristic of β-sheet, in their CD spectrum. We have shown that titration of CTX A3 with heparin, moni-

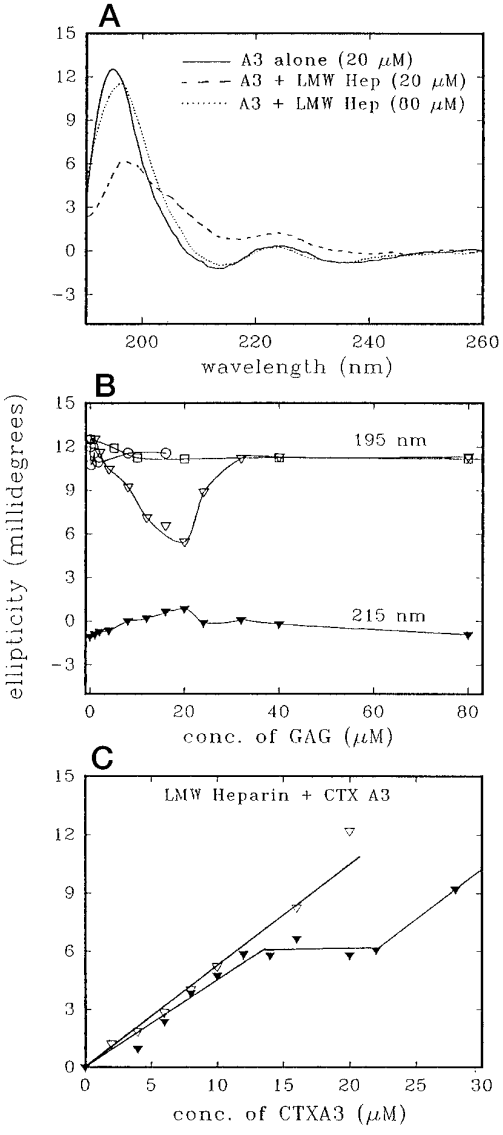

FIG. 3. **Binding behavior of several GAGs with CTX A3 as studied by CD measurement.** *A,* representative CD spectra of CTX A3 alone and in the presence of LMW heparin at the indicated concentrations. *B,* ellipticity of the protein at 195 and 215 nm (*open* and *closed symbols,* respectively) plotted as a function of concentration of GAG. *C,* reverse titration of CTX A3 *versus* LMW heparin; *open* and *closed symbols* represent the ellipticity at 195 nm of CTX alone and in the presence of LMW heparin, respectively. The symbols in *B* are as follows: *triangles*, LMW heparin; *circles*, hyaluronan; and *squares*, trisulfated heparin disaccharide. Almost no change in structure occurs for hyaluronan and heparin disaccharide. Also shown is the ellipticity of CTX A3 alone (*open symbols*, control) at 195 nm and in the presence (*closed symbols*) of LMW heparin (20 μM, constant, effective concentration) *versus* concentration of protein.

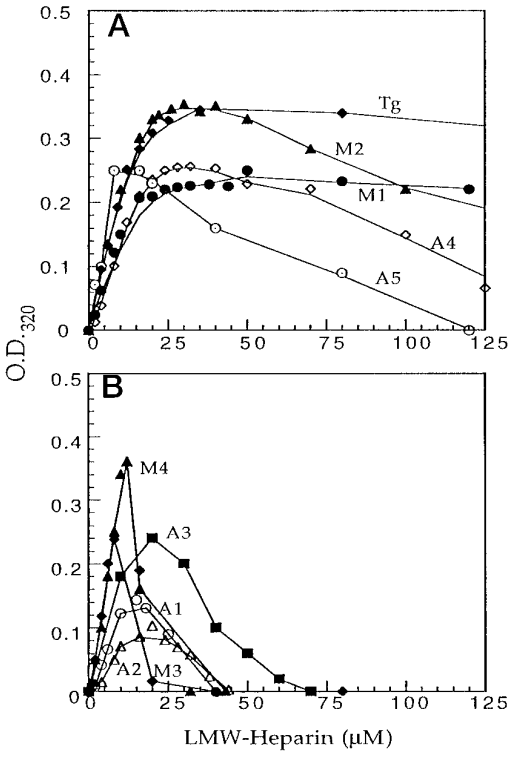

FIG. 4. **Interaction of CTXs with LMW heparin monitored by optical density (*OD*) measurements.** The reversal of turbidity is slow for toxins without Arg/Lys-6 (*A*) whereas is rapid for those containing Arg/Lys-6 (*B*).

tored by change in ellipticity at 195 nm, and ~215 nm, yields a two-phase curve, initial decrease in ellipticity ~195 nm followed by recovery of the same ellipticity at higher GAG concentrations (10). We have proposed that there exist two nonequivalent binding states and that the second binding state may be a manifestation of the aggregation of CTX molecules that accompanies saturated binding. To understand the details of binding, we performed similar titration of 10 CTXs.

All CTXs studied were found to bind to heparin; similar two-phase profile was obtained. Fig. 1, *A–C*, show, respectively, the representative spectra (*top panels*) and the plot of ellipticity *versus* heparin concentration (*bottom panels*) of CTXs A5, M4, and M1 (see Ref. 24 for details of classification). It can be seen that up to ~2 μM heparin, ellipticity ~195 nm decreases steadily as a function of heparin, reaches minimum, and increases again for higher heparin concentrations. Ellipticity ~215 nm exhibited similar change but with opposite sign (data not shown). Interestingly, in the presence of excess heparin, ellipticity of CTX A5 rises slightly higher than that for free form, whereas ellipticity of CTX M1 remains considerably lower than for free protein and is intermediate for CTX M4. Also, the effective concentration (amount of heparin required to produce maximum perturbation) varies from 2 to 2.8 μM for different toxins. The results of titration of 10 CTXs studied against HMW heparin are summarized in Fig. 2, *A* and *B*, and Table I.

For the sake of convenience of description we define ellipticity of free toxin as θ, that at maximum perturbation as θ_2, and that in the presence of excess heparin as θ_1 (Table I). In the change profile at ~195 nm, then, the point corresponding to maximum perturbation is $\Delta\theta_2$. The difference between θ_1 and θ, referred to here as $\Delta\theta_1$, denotes contribution to the magnitude of change of the first binding state, because this stronger binding state should predominate for excess heparin. The difference, $\Delta\theta_2 - \Delta\theta_1$, represents contribution of second binding state, assuming that the two sites are mutually independent.

As can be seen from Table I, CTX M1 and Tγ undergo maximum conformational change upon first binding (high $\Delta\theta_1$) while CTXs M2, M4, A3, and A5 undergo change upon second binding (high $\Delta\theta_2$ - $\Delta\theta_1$). Effective concentration of heparin required to produce maximum change in CTXs ($\Delta\theta_2$) also varies for different CTXs. That for CTX M4, A3, A2, A1, and M3 falls in the range of 1.8–2.0 μM, and that for CTXs M1, Tγ, M2, A5, and A4 varies from 2.4 to 3.0 μM. We have suggested that significant conformational change occurs due mainly to the aggregation of CTX–heparin complex around saturation; this indicates that the latter group prefers to remain in the aggregated state even when more heparin is added. It is interesting

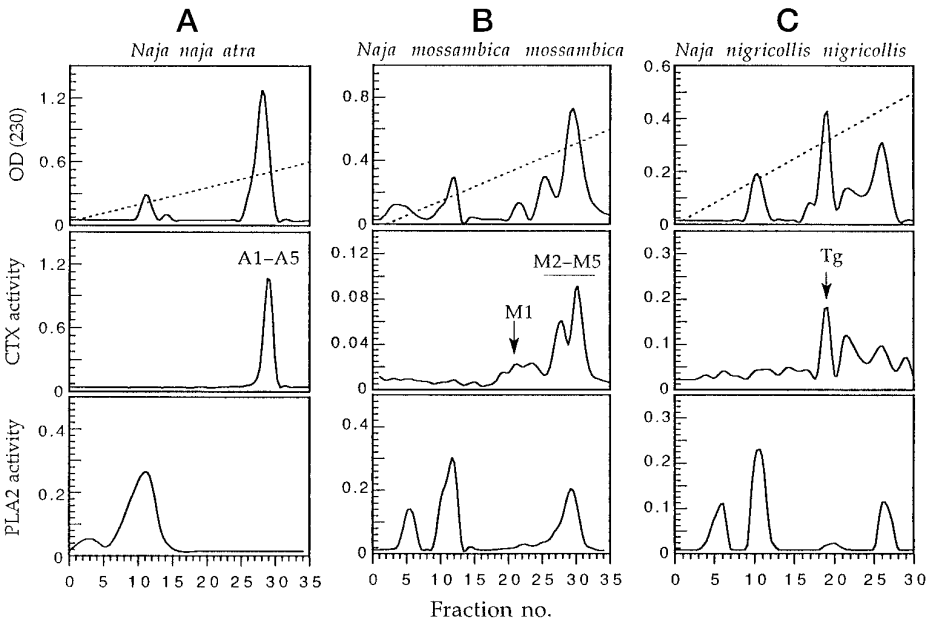

FIG. 5. **Determination of relative binding strength of CTXs from venom of *N. atra* (*A*), *N. mossambica* (*B*), and *N. nigricollis* (*C*) to heparin.** Eluted fractions were examined for protein concentration by monitoring absorbance at 230 nm (*upper panel*), CTX activity by monitoring fusion/aggregation of sphingomyelin vesicles (*middle panel*) and PLA2 activity by pH-stat (*lower panel*). PLA2 activity is presented as slopes of the respective curves of amount of NaOH required to titrate the fatty acid released from egg phosphatidylcholine vesicles as a function of time. The *dashed lines* in *upper panels* represent the NaCl gradient from 0 to 0.6 M.

to point out that the presence of basic residue appears to correlate with the suggested aggregation state of CTX-heparin complex. With the exception of CTX A4, the only CTX containing Arg at the N-terminal, all CTXs containing either Arg-6 or Lys-6 dissociate at lower effective heparin concentration of 1.8–2.0 μM (Tables 1 and 2). Additional evidence to support this interpretation can be obtained from turbidity data presented later.

Interaction of CTXs with LMW Heparin—HMW Heparin contains ~10 pentasaccharides and thus many CTX molecules may bind to heparin at maximum perturbation. This forced indulgence or molecular crowding may introduce constraints in the protein. To delineate the contribution of molecular crowding, we performed binding study using depolymerized heparin (average *M*r 3000, LMW heparin) which would be free of crowding. The composition of this heparin is heterogeneous (27); it contains saccharides of varying lengths while some sequences present in HMW heparin may be altogether absent in this lower homologue. This property of LMW heparin, however, allows identification of several trends that remain hidden with the higher homologue.

Shown in Fig. 3*A* are representative CD spectra of CTX A3 alone and in presence of LMW heparin. The profile of change in ellipticity *versus* concentration of LMW heparin is plotted in Fig. 3*B*. Like for HMW heparin, ellipticity ~195 nm decreased to minimum at 20 μM heparin and resumed that of free protein at 80 μM heparin. Similar titration with trisulfated heparin disaccharide and hyaluronan, the GAG lacking sulfate, revealed that no change occurred in CTX A3 (Fig. 3*B*; see also Ref. 10). This indicates that a sulfated stretch longer than disaccharide is required for binding.

The reversibility of binding and regaining of ellipticity of CTX A3 at higher concentrations of LMW heparin are similar to that for HMW heparin. The effective concentration of LMW derivative, 20 μM, however, is ~10-fold higher than for HMW heparin. But the difference in their molecular weights is ~5-fold. The higher effective concentration for LMW heparin can be explained by the absence in this sulfated oligosaccharide of some sequences required for binding. We therefore performed similar titration in the reverse order to gain insight into binding.

LMW heparin (20 μM, constant, effective concentration) was titrated against CTX A3. Fig. 3*C* shows profile of ellipticity of CTX A3 in absence (*open symbols*) and presence (*closed symbols*) of the heparin *versus* concentration of CTX A3. It can be seen that upon addition of CTX A3 to heparin, the ellipticity rises steadily, and the rise is comparable to that for free protein (compare with control), which indicates that this binding causes no perturbation. Since heparin is present in excess here, this binding can be considered to be strong. After addition of 12 μM of CTX A3; however, further addition of toxin does not cause an increase in ellipticity, which instead remains constant until 20 μM. This indicates that maximum perturbation occurs around here since the added CTXs do not contribute to CD signal as expected. Optical density measurement suggests that the turbidity increases abruptly from 0.02 to 1.0 from 12 to 20 μM protein (data not shown). Beyond 20 μM, the ellipticity again rises sharply and the rise is comparable to that of free CTX A3 (compare with control), but the turbidity remains at around 1.0. This indicates that binding is saturated after 20 μM and that most conformational change occurs due to aggregation of CTX–heparin complex. In conclusion, CTX A3 binds similarly to LMW and HMW heparin. The effective binding sites available in LMW heparin are, however, less than those of HMW heparin even after normalizing with their respective molecular weights.

We then performed titration of 10 CTXs with LMW heparin and monitored change in ellipticity. The results are summarized in Fig. 2, *C* and *D* to allow comparison with similar experiments done with HMW heparin (Fig. 2, *A* and *B*). For convenience of our discussion, the results obtained for HMW heparin are classified according to the difference in their effective charge, whereas those obtained for LMW heparin are classified according to the differences in their degree of conformational change. It can be seen that some CTXs undergo small structural perturbation (Fig. 2*C*), while others undergo large change in ellipticity (Fig. 2*D*) upon binding to LMW heparin. A similar result can also be observed for HMW heparin, but the interpretation is complicated because of the combined effect of molecular crowding and aggregation on the detected conformational change. The magnitude of change, *i.e.* the values of $\Delta\theta_2$, are listed in Table I. All S-type CTXs (CTX containing Ser-29) exhibit smaller conformational change, and CTX M2 and all P-type CTXs (CTX containing Pro-31) exhibit larger conformational change (higher $\Delta\theta_2 - \Delta\theta_1$ or $\Delta\theta_1$). Comparison of their amino acid sequences indicates that Arg-28 and/or Lys-33 may

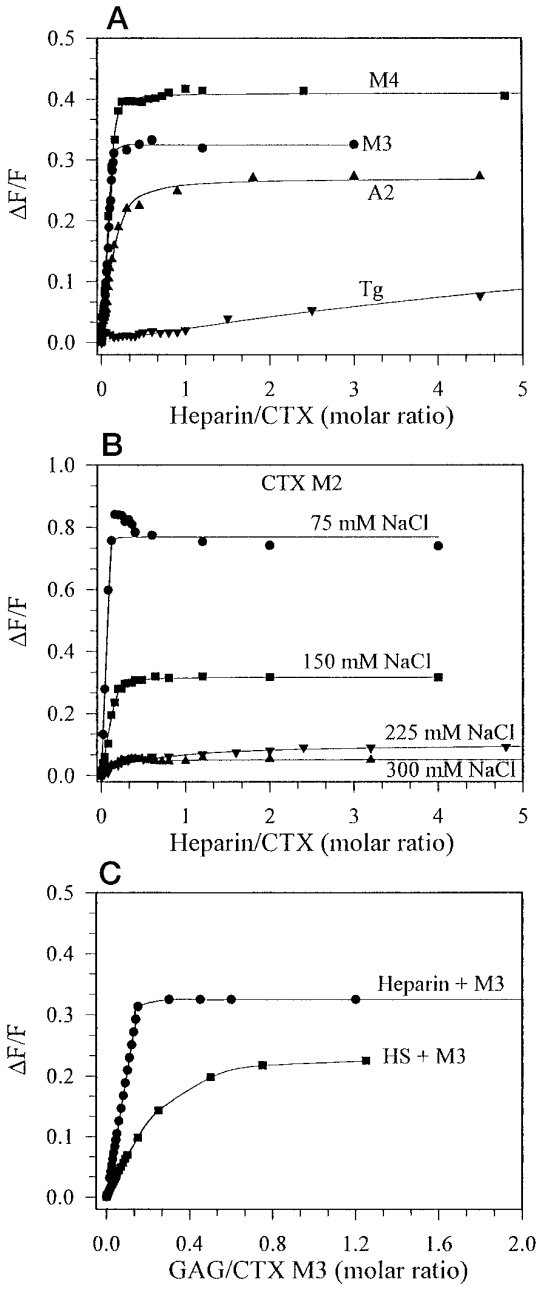

FIG. 6. **Change in fluorescence intensity of CTXs plotted against molar ratio of heparin/CTX.** *A,* binding curves for the indicated CTXs; *B,* binding curves at the indicated NaCl concentration in 10 mM phosphate at pH 7.4, for CTX M2; *C,* comparison of the binding of CTX M3 to heparin and heparan sulfate (*HS*). The change in anisotropy followed a similar trend (data not shown). Protein concentration was kept constant at 20 μM for Tyr- and 2 μM for Trp-containing CTXs.

enhance heparin-induced conformational change of the CTXs.

Comparison of $\Delta\theta_2$ values of CTXs with LMW and HMW heparin reveals that LMW heparin, on the same CTX, exerts smaller effect. This implies that molecular crowding arising out of the superstructure of the higher homologue contributes to structural perturbation of CTXs. Alternatively, the smaller effect of LMW heparin may be a manifestation of the absence in this polysaccharide of numerous sequences present in the HMW homologue. In summary, both molecular crowding and specific side chain interaction in the CTX-heparin complex play a role in heparin-induced CTX conformational changes.

Interestingly, binding of CTXs with LMW heparin was accompanied by change in turbidity of the solution. As shown in Fig. 4, the profile of turbidity change can be classified into two groups: one with slow decline (*panel A*) and the other with rapid decline (*panel B*) of turbidity, with increasing heparin concentration. This result strengthens our previous suggestion that CTXs containing Arg-6 or Lys-6 tend to dissociate easily when heparin is in excess. As reported previously (16), CTXs can be considered as slightly concave molecules with most of the basic residues lying on the concave side. Arg-6 or Lys-6, however, are located on the convex side of the surface and thus the absence of any ionic interaction helps dissociate the CTX/heparin complex at saturation. In other words, as this basic residue is exposed to the backside of CTX/heparin complex it is not involved in binding.

Binding Strength of CTXs with Heparin—Change in conformation and aggregation state of CTX–heparin complex help understand the mode of interaction, but do not reflect the binding strength. We therefore performed heparin-affinity chromatography and fluorescence spectroscopy binding measurements on the interaction of various CTXs with heparin to determine the relative binding strengths of the CTXs. The CTXs from *N. atra* bind to heparin with similar strength (Fig. 5*A*), whereas significant variation in the binding strength is found for CTXs from *N. mossambica* and *N. nigricollis* (Fig. 5, *B* and *C*). Interestingly, several PLA2 from *N. mossambica* and *N. nigricollis* bind to heparin stronger than most CTXs as indicated by the salt elution profiles.

To determine the dissociation constant of CTX–heparin complex, intrinsic fluorescence intensity of Tyr or Trp residues of CTX was measured as a function of heparin–CTX ratio. Fig. 6*A* shows representative fluorescence ($\Delta F/F$) profiles for CTX M4, M3, A2 and Tγ to indicate the variation in binding strength. Fitting of the data by non-linear least squares method based on Equation 1, presented in Material and Method section, allows determination of K_d and n. These values are listed in Table II, along with amino acid sequences of CTXs. Also shown is the salt concentration required to elute CTX from heparin affinity matrix, and the net positive charge content of CTXs.

The determined K_d values (Table II) of the toxins, and hence their binding strengths, vary by 4 orders of magnitude. The presence of basic residues near the tip of loop 2 appears to be most crucial in enhancing the binding strength. This observation confirms our previous conclusion based on the conformational change of CTXs that Lys-33 and/or Arg-28 are indeed involved in CTX–heparin interaction. It should be pointed out that although the relative binding strength determined by salt elution is in general consistent with that determined by spectroscopic method, distinct differences are clearly present, as for CTX M3 and M4. Conclusions of the binding strength of heparin binding proteins thus should not rely solely on the concentration of NaCl required to elute them from affinity matrices.

To demonstrate clearly that the different binding strengths reflect the involvement of basic residues, salt-dependence measurements of fluorescence intensity were performed on several selected CTXs. As can be seen in Figs. 6*B* and 7, binding of CTX with heparin exhibits significant salt-dependence. Surprisingly not all binding behavior of CTX can be understood in terms of macromolecule-polyelectrolyte theory, which holds good for most heparin binding proteins as suggested in earlier studies (28, 29). Specifically, a nonlinear dependence of log K_d with log [Na^+] can be seen for Tγ, a CTX that exhibits weak binding under physiological conditions (Fig. 7*A*).

A reasonable, linear salt-dependence of the binding is, however, detectable for CTX M2 (Fig. 7, *A* and *B*). Tγ and CTX M2 differ by only three amino acid residues at positions 29, 31 and 33 (Table II). Substitution of Ala-29, Pro-31, and Met-33 in Tγ by Gly-29, Ser-31, and Lys-33 in CTX M2 increases the binding

TABLE II

Correlation of sequence and net charge of CTXs with binding strength under physiological conditions

Dissociation constant, K_d, and the number of binding sites, n, were determined by nonlinear least squares fitting of fluorescence data. NaCl denotes the NaCl concentration required to dissociate the toxin from heparin affinity matrix. The net positive charge is calculated at pH 7.4. Conserved, basic residues are indicated by ● at the top of the respective columns; basic residues identified to be involved in heparin binding are highlighted in bold.

CTX	Amino acid sequences (10 / 20 / 30 / 40 / 50 / 60)	K_d	n	NaCl	Net positive charge
		μM		mM	
	● ● ● ● ●● ● ● ●				
M3	LKC-NKLIPI AYKTCPEGKN LCYKMMLAS**K** **K**-MVPVKRGC INVCPKNSAL VKYVCCSTDR CN	0.020	6.4	500	10
M2	LKC-NQLIPP FWKTCPKGKN LCYKMTM**R**GA S-**KV**PVKRGC IDVCPKSSLL IKYNCCNTDK CN	0.120	5.2	400	10
M4	LKC-NRLIPP FWKTCPEGKN LCYKMTMRLA P-**K**VPVKRGC IDVCPKSSLL IKYMCCNTNK CN	0.130	6.4	510	10
A5	LKCHNTQLPF IYKTCPEGKN LCFKATL**K**KF PL**K**FPVKRGC ADNCPKNSAL LKYVCCSTDK CN	0.25	9	460	9
A3	LKC-NKLVPL FYKTCPAGKN LCYKMFMVAT P-**K**VPVKRGC IDVCPKSSLL VKYVCCNTDR CN	1.42	9	440	9
A4	RKC-NKLVPL FYKTCPAGKN LCYKMFMVSN -LTVPVKRGC IDVCPKNSAL VKYVCCNTDR CN	2.55	8.2	420	9
A1	LKC-NKLIPI ASKTCPAGKN LCYKMFMMSD -LTIPVKRGC IDVCPKNSLL VKYVCCNTDR CN	2.68	8.3	440	7
A2	LKC-NKLVPL FYKTCPAGKN LCYKMFMVSN -LTVPVKRGC IDVCPKNSAL VKYVCCNTDR CN	3.83	5.4	420	8
M1	LKC-NQLIPP FWKTCPKGKN LCYKMTMRAA P-MVPVKRGC IDVCPKSSLL IKYMCCNTNK CN	135	8.0	320	10
Tg	LKC-NQLIPP FWKTCPKGKN LCYKMTMRAA P-MVPVKRGC IDVCPKSSLL IKYMCCNTDK CN	140	7.8	330	9

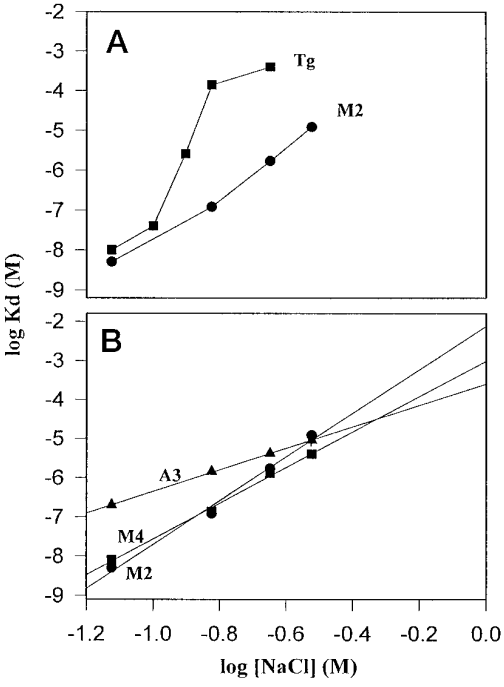

FIG. 7. **Ionic strength dependence of binding of representative CTXs with heparin.** A plot of log K_d as a function of log [NaCl] for CTX Tγ compared with M2 (*A*) and CTXs A3, M4, and M2 (*B*).

strength by three orders of magnitude in physiological buffer, although their binding strengths are similar in low salt buffer. The exact implication of this observation is not clear at present, but the results indicate clearly that the presence of Lys-33 is crucial for the specific binding of CTX with heparin.

As indicated in Table II, the binding strength of CTX is enhanced by one order of magnitude if another charged residue is present at position 28 (compare CTX M4 with A3). Salt dependence study further substantiates the suggestion that Arg-28 (or Lys-28, for CTX A5) is indeed involved in binding since the number of purely ionic interactions between the two species, Z, is higher for CTX M4. A similar conclusion can also be derived by comparing the salt-dependence curves of CTX A3 and M2 (Fig. 7*B*). It should be pointed out that salt dependence curves of dissociation constant determined for CTX M2 and M4 are not perfectly linear (Fig. 7*B*). Therefore, quantitative comparison based on macromolecule-polyelectrolyte theory may lead to substantially large values of Z than those predicted based on the charge difference (29). However, Arg-28 must also be involved in the binding of Lys-33 containing CTXs.

CTX M3 binds to heparin with exceptionally high strength. There is, however, no Lys-33 in the molecule. Instead, two Lys residues are located consecutively, at positions 31 and 32. Interestingly, the amino acid sequence of CTX M3 from 29 to 38 positions follows the so-called consensus sequence, xBBxxxBBx, of high affinity binding region of aFGF from amino acid position 126 to 135 (13, 30). We therefore conclude that the charge distribution near the tip of loop 2 region is important and is responsible for specific interaction between CTX and heparin.

We found that CTX M3 also binds to heparan sulfate (HS), the ubiquitous GAG on cell surface, with a dissociation constant of 6 μM (Fig. 6*C*). We have shown that HS binds to CTX A3 with K_d value of 16 μM in physiological buffer (10). The binding of CTX M3 to HS is thus about 3 times stronger than that of CTX A3, the difference between their heparin binding strength, on the other hand, is two orders of magnitude. Therefore, the strong association of CTX M3 with heparin can only be related to higher sulfation of heparin relative to HS.

Computer Modeling of the Molecular Interaction Between CTXs and Heparin—CTXs contain 9 discontinuous, basic residues (highlighted in Table II) capable of serving as binding sites for heparin. The three-dimensional structure of CTXs reveals that the protein exhibits significant polarization with the conserved basic residues, at positions 2, 24, 38, 46, 52 and 60, residing on the concave face of the three-finger disk-like structure, and the acidic residues opposite (16, 17). Since our experimental results suggest the involvement of Lys/Arg-28 and Lys-33 in the binding and they are known to be located on the same concave surface of the conserved basic residues, we performed computer modeling by docking the CTX molecules on the concave side of the molecule and carried out MD simulation to obtain detailed information of the binding at molecular level. The same conclusion as that based on the aggregation property of CTX/heparin complex was reached.

Shown in Fig. 8*A* are the stereo plots of the final energy-minimized structures of CTX A5-heparin complex generated by MD simulation. In addition to the two designated Lys at positions 28 and 33, heparin can also interact with CTX A5 via the side chains of Lys-24, Arg-38, Lys-46, Lys-52, and Lys-60 which are distributed as a positively charged band on the concave side of the molecules. Interestingly, these positively charged amino acid residues are conserved in all CTXs sequence available and are located at the same position as revealed by their three-dimensional structures. Electrostatic interaction, in the binding of CTX-heparin may be reinforced by this positively charged band structure. Possible electrostatic interactions be-

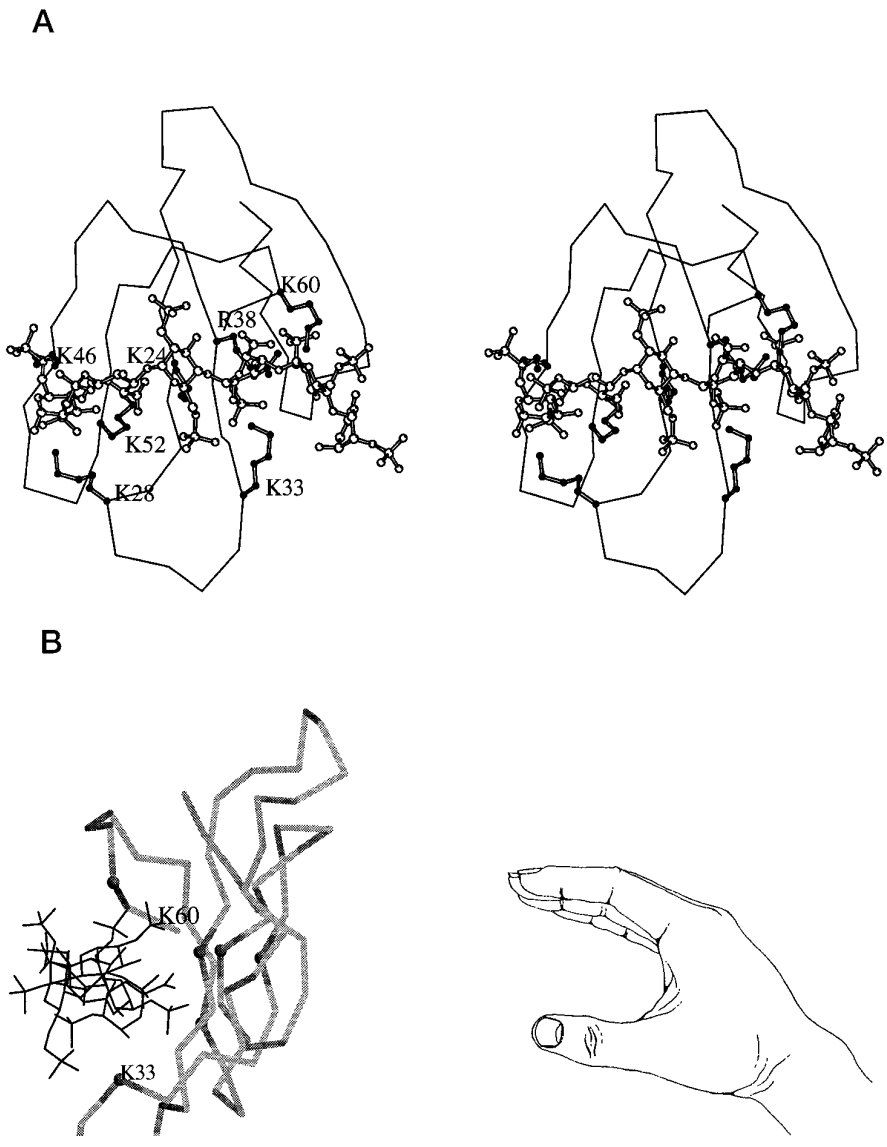

FIG. 8. **Molecular model for CTX/heparin interaction.** *A,* stereoplot of heparin binding to CTX A5. The complex represents the final energy-minimized structures generated by MD simulation of three-dimensional x-ray structure of CTX A5 (16). CTX is represented by wire-frame model of the C_α atoms, heparin is shown in ball-and-stick model (atoms in *open sphere*). The residues involved in polar interactions with heparin are also shown in ball-and-stick model with atoms in *filled sphere*. The figures were prepared using the program MOLSCRIPT (35). *B,* schematic diagram of the proposed model: the concave surface of the toxin is clearly seen in a side view of the C_α backbone. The conserved Lys residues, indicated by *dots*, lie around the base of the concave surface; and Lys-33, lying in the folds, extending away form the base, serves to reinforce binding of complementary charges. A cartoon drawing of the proposed model is also shown alongside; the complex can be conceived of as a hand enclosing the pentasaccharide. The Lys residues lie in the hollow of the palm, while Lys-33 can be considered to be the thumb; the pentasaccharide would bind only loosely were it not for the tightening afforded by the thumb.

tween CTXs and heparin are found to involve $-OSO_3^-$ group of the second, third, fourth, and sixth saccharides, $-NSO_3^-$ group of the second and sixth saccharides, and the $-CO_2^-$ group of the third and fifth saccharide. That only five saccharides participate in binding suggests that sulfated pentasaccharide may constitute an average binding unit as proposed by us recently (10).

DISCUSSION

We have herein studied binding of 10 CTXs with LMW and HMW heparin by spectroscopic and affinity chromatographic techniques. Correlation of the binding data with amino acid sequence of CTXs points to the importance of the distribution of charged residues at the tip of loop 2 of CTX. Despite the high homology these naturally occurring variants, basic toxins, display in their primary and three-dimensional structures, significant differences in their affinities for acidic heparin are found. Mere presence of conserved basic residues does not warrant high affinity heparin binding under physiological condition, although strong binding occurs under low salt condition, as observed for Tγ. High affinity heparin binding is only observed for CTXs containing specific basic residues near the tip of loop 2; however, the conserved, discontinuous, basic residues Lys-24, Arg-38, Lys-46, Lys-52, and Lys-60 are also involved in the interaction between CTXs and heparin due to electrostatic attraction.

The toxin contains two distinct cationic clusters: one primary recognition binding region comprising the conserved residues, which allows heparin to subsequently interact with another cationic cluster located at the tip of loop 2. This conclusion is consistent with recent study on the binding of heparin with other proteins. For instance, primary recognition site for heparin was concluded to lie at positions 122–137 of aFGF, although most other basic residues from other clusters are banded like an equator around the spherical FGF (30). Recently, the requirement of Lys and Arg residues outside the proposed pentasaccharide binding region for high affinity heparin binding is demonstrated for human antithrombin III (14, 31). High affinity binding structural motif of heparin can thus be considered to consist of two regions as illustrated in the schematic diagram, shown in Fig. 8*B*, based on the structure of β-sheet CTX.

Interestingly, of the total 9 conserved basic residues in CTXs, Lys-2 has previously been shown to stabilize the β-sheet structure (19), while Lys-12, Lys-18, and Lys-37 bind to phospholipids (17). Thus, all the 9 conserved basic residues in CTXs appear to have structural or functional roles, other than to simply increase solubility of this amphiphilic polypeptide. In this respect, CTX appears to be efficiently designed for inter-

TABLE III

Subtype classification of short chain neurotoxins (NTX) of cobra snake venom according to the putative heparin binding motif of cardiotoxins

Type of toxin[a]	Amino acid sequence	Source
P-type cardiotoxins		
	LKCHNTQLPF – IYKTCPEG KNLCFKATLK KFPLKFPVKR GCADNCPKNS ALL ***K*** YVCCST DKCN-	*N. atra*, CTX A5
K-type neurotoxins		
	10 20 30 40 50 60 65	
	LECHNQQSSQ APTTKTCSGE -TNCY**K**KWWS -DH**R**GTIEE**R** GC–GCP**K**V**K** PGV ***K*** LNCCRT D**R**CNN	*N. Philippinensis NTX toxin*
	LECHNQQSSQ PPTTKTCPGE -TNCY**K**KVWR -DH**R**GTIIE**R** GC–GCPTV**K** PGI ***K*** LNCCTT D**K**CNN	*N. nigricollis*, NTX toxin α
	MECHNQQSSQ PPTTKTCPGE -TNCY**K**KQWS -DH**R**GTIIE**R** GC–GCPSV**K** KGV ***K*** INCCTT D**R**CNN	*N. melanoleuca*, NTX toxin d
E-type neurotoxins		
	LECHNQQSSQ TPTTGCSGGE -TNCY**K**KRW**R** -DH**R**GYRTE**R** GC–GCPSVK NGI ***E*** INCCTT D**R**CNN	*N. atra*, cobrotoxin
	LECHNQQSSE PPTTRCSGGE -TNCY**K**KRW**R** -DH**R**GYRTE**R** GC–GCPTVK KGI ***E*** LNCCTT D**R**CNN	*N. mossambica*, NTX toxin I
	LECHNQQSSQ PPTTKTCPGE -TNCY**K**KRW**R** -DH**R**GSITE**R** GC–GCPSVK KGI ***E*** INCCTT D**K**CNN	*N. nivea*, NTX toxin δ
	MICYKQQSLQ FPITTVCPGE -KNCYKKQWS -GH**R**GTIIE**R** GC–GCPSVK KGI ***E*** INCCTT D**K**CNR	*N. haje (annulifera)*, NTX toxin CM-10
G-type neurotoxins		
	MICHNQQSSQ RPTIKTCPGE TNCY**K**KRW**R** -DH**R**GTIIE**R** GC–GCPSV**K** KGV ***G*** IYCCKT D**K**CNR	*N. nivea*, NTX toxin β
	MICHNQQSSQ PPTIKTCPGE -TNCY**K**KQW**R** -DH**R**GTIIE**R** GC–GCPSV**K** KGV ***G*** IYCCKT D**K**CNR	*N. haje (haje)*, NTX toxin CM-10a
	MICHNQQSSQ PPTIKTCPGE -TNCY**K**KRW**R** -DH**R**GTIIE**R** GC–GCPSV**K** KGV ***G*** IYCCKT N**K**CNR	*N. haje (annulifera)*, NTX toxin CM-14
Consensus sequence		
	--C--- ----------C- -----C-**K**--W**R** -DH**R**-----**R** -C--C---K --- ***X*** --CC-- -**K**C--	

[a] The amino acid sequences of neurotoxins are taken from Ref. 31. Neurotoxins containing a Lys, Glu, or Gly amino acid at position 54 are tentatively defined as K-type, E-type, and G-type neurotoxins, respectively. The basic amino acid residues constituting putative heparin binding sites of CTX A5 and NTXs are highlighted (bold) and the numbering of their amino acid positions is shifted by two relative to that shown in Table II.

action with membrane components. The small dimension of CTX molecules (35 × 24 × 15 Å) (16) also indicates that it is probably one of the smallest polypeptides with well defined three-dimensional structure that interacts with sulfated oligosaccharide of heparin.

The conserved basic residues of CTXs implicated in heparin binding follow the order -B-X_{2n-1}-B-, where X is any residue and B is basic residue. Thus, discontinuous basic residues separated by odd number of any residue appears to constitute a suitable heparin binding motif in the β-sheet proteins studied. Although such discontinuous distribution is in contrast to clustering of basic residues in other heparin-binding protein with α-helix (13), it is not surprising in view of the alternating distribution of amino acid side chain in β-sheet polypeptides. Therefore, suitable structural binding motif of heparin can be identifiable, as illustrated in the presently proposed model of CTX-heparin interaction, for heparin binding protein with known three-dimensional structure.

A similar spatial distribution of conserved basic residues is also found in the structurally related three finger venom neurotoxins (NTXs) that bind avidly to acetylcholine receptors (Table III). Sequence alignment of 10 NTXs (also from cobra venom) reveals that all the five basic residues are localized on the same face of NTX molecule and may thus be accessible if guided by the specific recognition site of NTX, -W-*X*-D-H- (32), which are known to be near the tip of loop 2 (shown in Table III). This distribution of basic residues in NTXs suggests that they may use the binding mode similar to CTX to bind to acetylcholine receptor. It has recently been demonstrated that modification of Arg residues of loops 2 and 3 and C-terminal of NTX from King cobra caused a 90–92% decrease in lethality and abolished acetylcholine receptor binding. These results indicate that in addition to the established recognition site of loop 2, other cationic residues of different regions are also important in receptor binding and lethality (33, 34). Amino acid sequences in NTX show distinct distribution of charged residues from position 50 to 60 (Table III). Three different classes of NTXs, K-type, E-type and G-type, containing Lys-54, Glu-54 and Gly-54, respectively, emerge upon sequence alignment. It is suggested that substitution of acidic or neutral residues at this position may further modulate the specific interaction of NTX with its receptor.

The fact that CTXs and several PLA2 exhibit significantly different binding strength to heparin (Fig. 5) contains important biological implications in that such binding to heparin-like oligosaccharides may serve to concentrate proteins with different properties at the site of action. It is known that PLA2 and CTXs act synergistically on many cell systems (21, 22). Binding of human PLA2 type II to proteoglycans causes differential effect on its enzymatic activity as demonstrated recently (8), an indication that heparin modulates the toxicity of these polypeptides. Since both toxins have different targets and since all the known targets of these toxins lie at the membrane, future study of the interplay between CTX and PLA2 near the membrane surface may provide information on GAG-guided protein action on membranes.

Acknowledgments— W. Wu thanks Professors C. Ho and J. Prestegard for initial discussion on interaction of CTXs with carbohydrates.

REFERENCES

1. Salmivirta, M., Lidholt, K., and Lindahl, U. (1996) *FASEB J.* **10,** 1270–1279
2. Jackson, R. L., Busch, S. J., and Cardin, A. D. (1991) *Physiol. Rev.* **71,** 481–539
3. Lindahl, U., Lidholt, K., Spillman, D., and Kjellen, L. (1994) *Thromb. Res.* **75,** 1–32
4. Linhardt, R. L. (1991) *Chem. & Ind.* 45–50
5. Yanagishita, M., and Hascall, V. C. (1992) *J. Biol. Chem.* **267,** 9451–9454
6. Ruoslathi, E., and Yamaguchi, Y. (1991) *Cell* **64,** 867–869
7. Rosenfeld, L., and Danishefsky, I. (1987) *Biochemistry* **12,** 639–649
8. Sartipy, P., Johansen, B., Camejo, G., Rosengren, B., Bondjers, G., and Hurt-Camejo, E. (1996) *J. Biol. Chem.* **271,** 26307–26314
9. Lomonte, B., Moreno, E., Tarkowski, A., Hanson, L. A., and Maccarana, M. (1994) *J. Biol. Chem.* **269,** 29867–29873
10. Patel, H. V., Vyas, A. A., Vyas, K. A., Liu, Y.-S., Chiang, C-M., Chi, L-M., and Wu, W. (1997) *J. Biol. Chem.* **272,** 1484–1492
11. Spillman, D., and Lindahl, U. (1994) *Curr. Opin. Struct. Biol.* **4,** 677–682
12. Cardin, A. D., and Weintraub, H. J. R. (1989) *Atherosclerosis* **9,** 21–32
13. Margalit, H., Fischer, N., and Ben-Sasson, S. A. (1993) *J. Biol. Chem.* **268,** 19228–19231
14. Kridel, S. J., Chan, W. W., and Knauer, D. J., (1996) *J. Biol. Chem.* **271,** 20935–20941
15. Faham, S., Hileman, R. E., Fromm, J. R., Linhardt, R. J., and Rees, D. C. (1996) *Science* **271,** 1116–1120
16. Sun, Y.-J., Wu, W., Chiang, C.-M., Hsin, Y.-A., and Hsiao, C.-D. (1997) *Biochemistry*, **36,** 2403–2413
17. Bilwes, A., Rees, B., Moras, D., Ménez, R., and Ménez, A. (1994) *J. Mol. Biol.* **239,** 122–136
18. Singhal, A. K., Chien, K.-Y., Wu, W., and Rule, G. S. (1993) *Biochemistry* **32,** 8036–8044

19. Chiang, C.-M., Chang, S.-L., Lin, H.-J., and Wu, W. (1996) *Biochemistry* **35,** 9177–9186
20. Rees, B., and Bilwes, A. (1993) *Chem. Res. Toxicol.* **6,** 385–406
21. Dufton, M. J., and Hider, R. C. (1991) in *Snake Toxins* (Harvey, A. L., ed) pp.259–302, Pergammon Press Inc., Elmsford, NY
22. Fletcher, J. E., and Jiang, M.-H. (1993) *Toxicon* **31,** 669–695
23. Chien, K.-Y., Huang, W.-N., Jean, J.-H., and Wu, W. (1991) *J. Biol. Chem.* **266,** 3252–3259
24. Chien, K.-Y., Chiang, C.-M., Hseu, Y.-C., Vyas, A. A., Rule, G. S., and Wu, W. (1994) *J. Biol. Chem.* **269,** 14473–14483
25. Wüster, W. (1996) *Toxicon* **34,** 399–406
26. Fryklund, L., and Eaker, D. (1975) *Biochemistry* **14,** 2865–2871
27. Arakawa, T., Wen, J., and Philo, J. S. (1994) *Arch. Biochem. Biophys.* **308,** 267–273
28. Olson, S. T., Halvorson, H. R., and Bjork, I. (1991) *J. Biol. Chem.* **266,** 6342–6352
29. Thompson, L. D., Pantoliano, M. W., and Springer, B. A. (1994) *Biochemistry* **33,** 3831–3840
30. Wong, P., Hampton, B., Szylobryt, E., Gallagher, A. M., Jaye, M., and Burgess, W. H. (1995) *J. Biol. Chem.* **270,** 25805–25811
31. Meagher, J. M., Huntington, J. A., Fan, B., and Gettins, P. G. W. (1996) *J. Biol. Chem.* **271,** 29353–29358
32. Endo, T., and Tamiya, N. (1991) in *Snake Toxins* (Harvey, A. L., ed) pp. 165–222, Pergammon Press Inc., Elmsford, NY
33. Lin, S. R., Chi, S. H., Chang, L. S., Kuo, K. W., and Chang, C. C. (1995) *Biochem. J.* **297,** 297–301
34. Lin, S. R., Chi, S. H., Chang, L. S., Kuo, K. W., and Chang, C. C. (1996) *J. Protein Chem.* **15,** 95–101
35. Kraulis, P. J., (1991) *J. Appl. Crystallogr.* **24,** 946–950